

# Mirror-Aware Neural Humans

Daniel Ajisafe<sup>1</sup> James Tang<sup>1</sup> Shih-Yang Su<sup>1</sup> Bastian Wandt<sup>1,2</sup> Helge Rhodin<sup>1</sup>

(dajisafe, shihyang, rhodin)@cs.ubc.ca, tangytob@student.ubc.ca, bastian.wandt@liu.se

<sup>1</sup>The University of British Columbia

<sup>2</sup>Linköping University

## Abstract

Human motion capture either requires multi-camera systems or is unreliable when using single-view input due to depth ambiguities. Meanwhile, mirrors are readily available in urban environments and form an affordable alternative by recording two views with only a single camera. However, the mirror setting poses the additional challenge of handling occlusions of real and mirror image. Going beyond existing mirror approaches for 3D human pose estimation, we utilize mirrors for learning a complete body model, including shape and dense appearance. Our main contributions are extending articulated neural radiance fields to include a notion of a mirror, making it sample-efficient over potential occlusion regions. Together, our contributions realize a consumer-level 3D motion capture system that starts from off-the-shelf 2D poses by automatically calibrating the camera, estimating mirror orientation, and subsequently lifting 2D keypoint detections to 3D skeleton pose that is used to condition the mirror-aware NeRF. We empirically demonstrate the benefit of learning a body model and accounting for occlusion in challenging mirror scenes. The project is available at: <https://danielajisafe.github.io/mirror-aware-neural-humans/>.

## 1. Introduction

Estimating detailed 3D geometry of a moving person from a single video is a long-standing goal. Learning-based solutions can succeed when trained on 3D labels from the target domain or when multiple 2D views are available for supervision [30, 33, 37–39, 44, 48]. However, multi-view capture is expensive and tedious to calibrate, and hence, the diversity of existing datasets and associated machine learning solutions are limited to mainstream activities and environments.

We propose a test-time optimization method for reconstructing a generative body model entailing pose, shape, and appearance using a single camera and a mirror and starting from 2D pose without any 3D labels nor large-scale dataset.

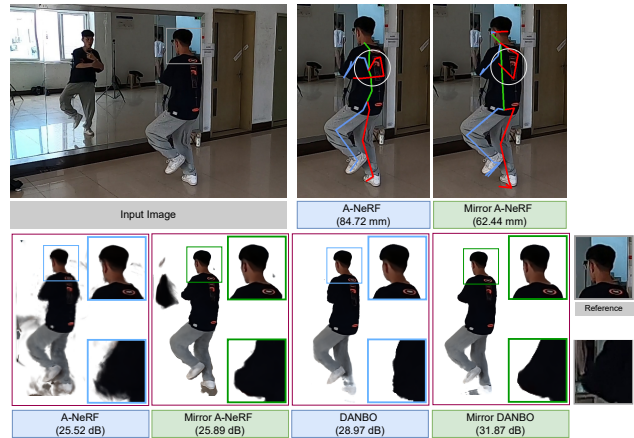


Figure 1. **Pose refinement and image quality.** Given an image with mirror (top left) our mirror-based method reconstructs 3D pose and shape that is more accurate than the baselines (A-NeRF [42] and DANBO [43]) not supporting the mirror, both in terms of the 3D pose metric PA-MPJPE (top row, e.g., corrected arms), and in image quality PSNR (bottom row, e.g., reconstructed earphone and left elbow).

The mirror setting is practical: First, mirrors are readily available in urban environments and provide a second view for accurate reconstruction without requiring multi-camera recording and temporal synchronization. Second, off-the-shelf 2D estimators generalize well since diverse training images are easily annotated by clicking 2D joint locations. Previous works [8, 27] leveraged reflections in mirrors for better human pose reconstruction. However, neither of them model shape and appearance in detail. In addition, the model proposed in [8] needs a 3D pose estimator as prior, potentially limiting their approach to motions close to the training set.

Alternatively, 3D body models have been learned from monocular video. However, existing approaches either use a shape prior, such as a scan of the person [15], a parametric body model [2], restrict motions to be simple [54], or require initialization with a prior 3D estimator [42, 43, 52].

This restricts the possible motion, shape, and appearance complexity. By contrast, our mirror setting is simple, enabling anyone to collect 3D data of their target domain.

Our approach for learning *Mirror-Aware Neural Humans* makes no prior assumption about the body shape by building upon the open-source articulated neural radiance fields (NeRF) models [42, 43], which require only the joint angles of a skeleton as input. We estimate this skeleton fully automatically and without prior assumptions on the 3D poses using an automatic mirror calibration (Step 1) and mirror-based 2D to 3D pose lifting (Step 2), thereby avoiding the use of 3D pose estimators that struggle with occlusions and extreme poses. Our core contributions are as follows:

- Designing a robust algorithm that estimates mirror position and orientation, and 3D skeleton model with bone-relative coordinates suitable for neural body models.
- A layered mirror model, extending NeRF with occlusion handling of the mirror image by the real person.
- Developing a complete motion capture system for reconstructing human pose, shape, and appearance from mirror images, and making the source code available at: <https://github.com/danielajisafe/Mirror-Aware-Neural-Humans>.

## 2. Related Work

### Self- and weakly supervised learning approaches.

Weakly supervised 3D pose estimators typically leverage small-scale 3D pose datasets and combine them with additional 2D data [4, 14, 16, 24, 47, 49, 50, 56]. Others utilize neural networks that are pretrained on the 3D lifting task and transfer them to another dataset [10–12, 28, 29, 35]. Such weak supervision transfers better to unseen poses. However, they still make the assumption that training poses are close to the training set. A different approach is using multi-view supervision to learn an embedding of 3D poses [30, 33, 37–39, 44] or learn the 3D reconstruction step directly from multi-view images [20, 21, 40, 48]. While promising, they still require multiple temporally synchronized cameras for training. In contrast, using mirrors in a scene gives the unique advantage of having a pair of synchronized views with a single recording device.

**Mirror geometry and calibration.** Mirrors have a long history in visual computing on which Reshetouski et al. [36] provide a good overview. We take inspiration from methods [1, 17, 31, 45] employing mirrors for camera calibration and 3D reconstruction of rigid objects, to enable calibration and reconstruction of moving humans. Alternatively, Yin et al. [55] reconstructs arbitrary objects in mirror-like surfaces but do not show any application for humans.

**Mirror-based human pose estimation.** Nguyen et al. [32] use mirrors to reconstruct human point clouds, but require a depth camera together with two or multiple mirrors. To the best of our knowledge, the most related work that re-

constructs human pose and body shape with a single mirror is from Fang et al. [8]. They provide an optimization-based approach that utilizes mirror symmetry constraints for predicting 3D human pose and mirror orientation. While attaining high accuracy, they require as input an initial 3D pose estimate from a pretrained neural network that cannot generalize well to unseen poses. Moreover, their best results are attained using manually annotated vanishing lines on the mirror boundary [7]. By contrast, we use a purely geometric approach to optimize for 3D keypoints without requiring any 3D pose estimator or mirror annotation (with the neural network only modeling shape and appearance), by jointly optimizing for the bone orientation and building upon recent work on estimating camera position and ground plane using the motion of people in the scene [9, 46]. Similar to prior approaches [8, 27], we estimate 3D human keypoints as a solution to an optimization problem between two sets of mirrored 2D keypoints. By contrast, Liu et al. [27] optimize for 3D joint coordinates which can lead to incorrect pose sequences where, for example, bone lengths vary over time, and orientation remains ambiguous. Fang et al. [8] restrict motions to be close to sequences previously captured by pre-trained detectors, and none of these methods take detailed reconstruction of shape and appearance into account.

## 3. Method

Our goal is to reconstruct a dense neural body model from a single video with only sparse 2D detections as input, using the mirror as a second view to impose multi-view constraints. The difficulty lies in reconstructing such dense representation from only sparse and noisy 2D labels, with an unknown mirror and camera configuration. By contrast to classical multi-view settings, mirror observations add the difficulty of the real person occluding the mirror image. To overcome these difficulties, our method goes from sparse to fine details in three steps, as sketched in Figure 3.

For each step we use a suitable representation for the mirror geometry, each mathematically equivalent yet implying a different implementation. Figure 2 visualizes the three forms. *Case I:* A single camera  $c$  with light rays reflecting on the mirror plane  $\pi$ . *Case II:* The mirror image stemming from a *virtual camera*  $\bar{c}$  opposing the real camera  $c$ . *Case III:* A *virtual person*  $\bar{p}$  opposing the real person  $p$ , both viewed from the real camera  $c$ .

### 3.1. Camera and Mirror Initialization (Step 1)

We start from a video that shows a person moving in front of a mirror and use off-the-shelf pose detectors [6, 53] to obtain 2D pose estimates  $\mathbf{q}^{(t)} \in \mathbb{R}^{2 \times J}$  for every input frame  $\mathbf{I}_t$  and all  $J$  joints. As we assume the mirror is orthogonal to the ground, mirror and real images appear to be standing on the same ground plane and existing solutions to using the human as calibration object apply. We use a

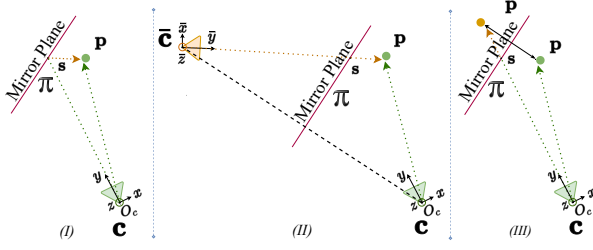


Figure 2. **Models for the mirror reflection.** In the first case, the rays go from the real camera  $c$  up to the mirror plane  $\pi$  intersecting at location  $s$ , then to the real person  $p$  after a mirror reflection. In the second case, the real person  $p$  is viewed from a virtual camera  $\bar{c}$  forming a virtual image. In the third case, the person location is mirrored to  $\bar{p}$  and light rays go straight from camera  $c$  to  $\bar{p}$ .

variant of single-view distance estimation [9] as described in method [3] that yields focal length  $f$  and ground plane normal  $n_g$ .

**Associating real and mirror poses.** Pose detectors are not aware of the mirror and therefore treat each person independently. We associate the pose with the largest neck-to-pelvis distance as the real person, utilizing that the person viewed through the mirror is farther away and hence smaller in the perspective camera. This association is also required for flipping the left and right side of the mirrored 2D pose to account for the mirror operation. Figure 4 shows this relationship and the degradation when misaligned.

**Mirror geometry initialization.** Under the assumption that the mirror normal is orthogonal to the ground plane normal, we obtain the 3D location of the real person and mirrored person using *Case III* (see Figure 2). We project their 2D ankle locations  $\mathbf{q}_{\text{ankle}}$  onto the estimated ground plane by reversing the projection

$$\mathbf{q} = \mathbf{K}\mathbf{p}, \text{ where } \mathbf{K} = \begin{pmatrix} f & 0 & o_1 & 0 \\ 0 & f & o_2 & 0 \\ 0 & 0 & 1 & 0 \end{pmatrix}, \quad (1)$$

with  $(o_1, o_2)$  the image center and  $f$  the estimated focal length. The mirror normal  $\mathbf{n}_m \in \mathbb{R}^3$  is then the vector from real  $\mathbf{p}_{\text{ankle}}$  to mirror  $\bar{\mathbf{p}}_{\text{ankle}}$ ,

$$\mathbf{n}_m = \frac{\mathbf{p}_{\text{ankle}} - \bar{\mathbf{p}}_{\text{ankle}}}{\|\mathbf{p}_{\text{ankle}} - \bar{\mathbf{p}}_{\text{ankle}}\|}. \quad (2)$$

The mirror location is the midpoint,  $\mathbf{m} = (\mathbf{p}_{\text{ankle}} - \bar{\mathbf{p}}_{\text{ankle}})/2$ . For increased robustness, we average over all frames.

### 3.2. 2D to 3D Pose Lifting (Step 2)

In this section, we use the notion of a virtual camera (*Case II*) positioned behind the mirror as shown in Figure 2. Following [23, 41], we derive the virtual camera through the matrix  $\mathbf{A}$  that mirrors points across the mirror plane,

$$\mathbf{A} = \begin{bmatrix} 1 - 2n_x^2 & -2n_y n_x & -2n_z n_x & -2n_x d \\ -2n_y n_x & 1 - 2n_y^2 & -2n_y n_z & -2n_y d \\ -2n_z n_x & -2n_y n_z & 1 - 2n_z^2 & -2n_z d \\ 0 & 0 & 0 & 1 \end{bmatrix}, \quad (3)$$

with  $\mathbf{n}_m = [n_x, n_y, n_z]$  the mirror normal and  $d$  the distance between camera and mirror. Both quantities are from Step 1. By defining the real camera to be at the origin pointing along the  $z$ -axis,  $\mathbf{A}$  maps points from the real to the virtual camera. The orientation of the virtual camera is hence  $\bar{\mathbf{R}} = \mathbf{A}_{3 \times 3}^\top$ , the inverse of the top-left part of  $\mathbf{A}$ , and camera position  $\bar{c} = -2\mathbf{n}_m d$ , is the negative of the last column of  $\mathbf{A}$ . Note that  $\bar{\mathbf{R}}$  is from the orthogonal group  $O(3)$  as it includes a reflection component given by the mirror.

**Mirror skeleton representation.** To be able to reconstruct not only the position but also the orientation of limbs, we represent  $\mathbf{p}^{(t)}$  with a skeleton parameterized by joint rotations  $\theta_i^{(t)} \in \mathbb{R}^6$ , using the 6D rotation parameterization of [57], bone lengths  $\ell \in \mathbb{R}^J$ , and the 3D pelvis position  $\mathbf{p}_{\text{pelvis}}^{(t)} \in \mathbb{R}^3$  (the root position). Forward kinematics gives

$$\mathbf{p}_j^{(t)} = \prod_{i \in \mathcal{N}(j)} \mathbf{T}_i \begin{bmatrix} \mathbf{0} \\ 1 \end{bmatrix} + \mathbf{p}_{\text{pelvis}}^{(t)}, \mathbf{T}_i = \begin{bmatrix} \mathbf{M}(\theta_i^{(t)}) & \ell_i \mathbf{v}_i \\ \mathbf{0} & 1 \end{bmatrix}, \quad (4)$$

with  $\mathbf{v}_i^{\text{ref}} \in \mathbb{R}^3$  the  $i$ th bone vector (parent to child vector) in a reference pose,  $\mathbf{M}(\theta_i^{(t)})$  the joint rotation computed from  $\theta_i^{(t)}$ , and  $\mathcal{N}(j)$  the ancestors of  $j$  in the kinematic chain. In the following, we optimize these parameters by using different constraints on the mirror scene including the pose, feet, and bone orientation.

**3D pose initialization.** Unlike prior work using joint locations [27], the bone rotation estimation we require is prone to local minima. To overcome this, we initialize with a constant standing pose adapted from the first frame of H36M [18, 19] at the estimated  $\mathbf{p}_{\text{ankle}}$ , rotated in  $45^\circ$  steps from  $0^\circ$  to  $360^\circ$  degrees as shown in Figure 5, and select the rotation with the lowest reconstruction error before optimization.

**3D pose optimization.** Using the virtual camera (*Case II* above), the optimization of the 3D pose  $\mathbf{p}$  under mirror constraints becomes a classical multi-view reconstruction problem. We optimize the skeleton parameterization  $\theta$  that,

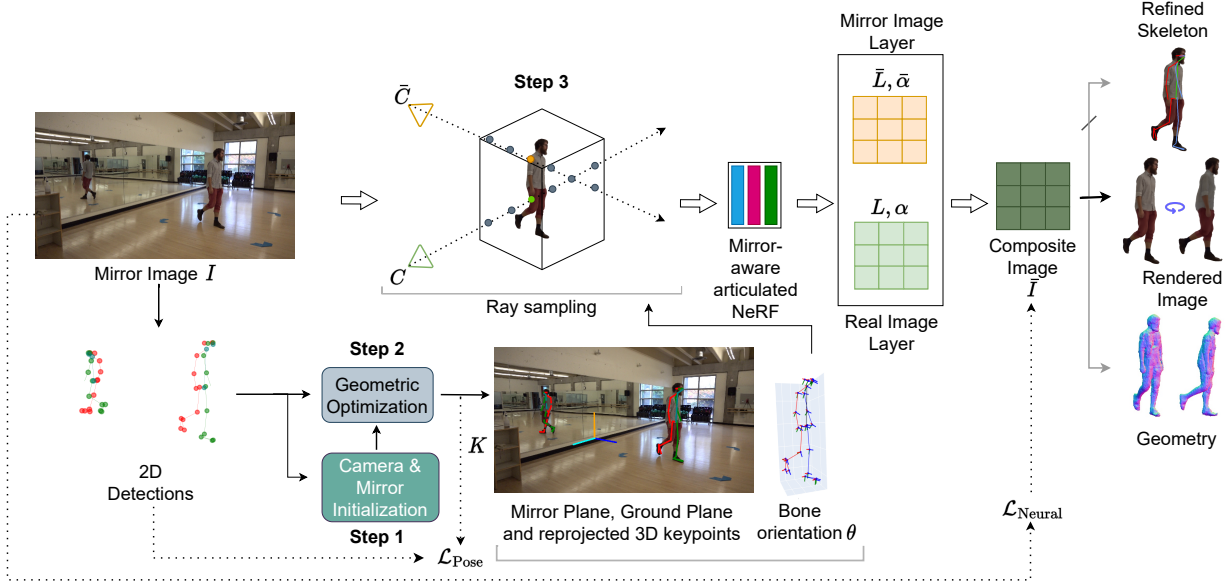


Figure 3. We start from a mirror image with an unknown mirror geometry. With only 2D detections and suitable assumptions, we reconstruct the mirror plane, ground plane, and 3D keypoints in Step 1 and Step 2. Our optimization yields bone orientation that is crucial for integrating NeRF with the mirror-based reconstruction. The final Mirror-aware Neural Human is learned via layered composition of mirror and real images in Step 3 and yields improved body pose, shape, and appearance quality.



Figure 4. **Real and mirror pose assignment.** Our algorithm distinguishes the real from the virtual person using pelvis-to-neck distance. With the right assignment and correct flipping, cases of collapsed poses (left) are corrected (right).

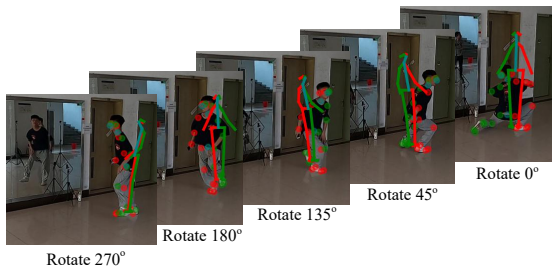


Figure 5. **3D pose initialization.** by measuring the error between initial re-projections (lines forming skeleton) and 2D detections (dots) to determine the optimal starting pose.

when reprojecting the associated 3D joint positions  $\mathbf{p}$  to the real and virtual cameras, minimizes the Euclidean distance

to real 2D pose  $\mathbf{q}$  and virtual 2D pose  $\bar{\mathbf{q}}$ ,

$$\mathcal{L}_p = \sum_t \|\mathbf{q} - \Pi(\mathbf{p}(\theta^{(t)}, \ell))\|^2 + \|\bar{\mathbf{q}} - \Pi(\mathbf{A}\mathbf{p}(\theta^{(t)}, \ell))\|^2 \quad (5)$$

with  $\mathbf{p}(\theta^{(t)}, \ell)$  the forward kinematic model and  $\Pi$  the perspective projection using  $\mathbf{K}$ . When 2D detection confidences are available, we use them as weights in Eq. 5.

**Smoothness and ground-plane constraints.** Frame-wise pose optimization leads to noisy reconstructions and inconsistent global orientations. To mitigate these, we encourage a constant velocity for location and joint angles across the video (for valid frames), referred to as *location* and *orientation smooth* in Eq. 6. To reduce floating, we utilize our ground plane estimate and constrain the lower feet by minimizing their distance to the ground plane, as described in Eq. 6 where  $\mathbf{f}_{gd} = (\mathbf{m} - \mathbf{f}_i)$ ,  $\mathbf{m}$  is the mirror location and  $\mathbf{f}_i$  is the closest foot (heel) to the ground. Lastly, we refine the mirror and ground normal,  $\mathbf{n}_m$  and  $\mathbf{n}_g$ , during optimization and enforce both quantities to be orthogonal.

We combine all additional objectives from above as

$$\begin{aligned} \mathcal{L}_{sto} = & \underbrace{\lambda_p \left\| \frac{d^2 \mathbf{p}(\theta^{(t)}, \mathbf{b})}{d_t^2} \right\|}_{\text{location smooth}} + \underbrace{\lambda_\theta \left\| \frac{d^2 \theta_k}{d_t^2} \right\|}_{\text{orientation smooth}} + \underbrace{\lambda_f (\mathbf{n}_g \mathbf{f}_{gd})^2}_{\text{feet constraint}} \\ & + \underbrace{(\mathbf{n}_g \mathbf{n}_m)^2}_{\text{orthogonality}} + \underbrace{(\|\mathbf{n}_m\|_2 - 1)^2}_{\text{mirror normal loss}} + \underbrace{(\|\mathbf{n}_g\|_2 - 1)^2}_{\text{ground normal loss}}, \quad (6) \end{aligned}$$



where  $\frac{d^2 \mathbf{p}(\theta^{(t)}, \mathbf{b})}{d_t^2}$  and  $\frac{d^2 \theta_k}{d_t^2}$  are the second-order derivatives for the joint locations and bone orientations for all frames  $t$ ,  $\mathbf{f}_{gd}$  is the vector from ground plane location to the lower feet of interest, and  $\lambda_p$ ,  $\lambda_\theta$ ,  $\lambda_f$  are hyper-parameters that balance the influence of the smoothness terms and the feet loss. Our final objective  $\mathcal{L}_{\text{pose}}$  is the sum of all individual terms,  $\mathcal{L}_{\text{Pose}} = \mathcal{L}_p + \mathcal{L}_{\text{sfo}}$ .

### 3.3. Neural Rendering and Refinement (Step 3)

With the 3D pose  $\mathbf{p}(t)$  reconstructed approximately for each pair of 2D detections  $\mathbf{q}(t)$  and  $\bar{\mathbf{q}}(t)$  in every frame of the video, we train a generative model  $G(\theta)$  conditioned on pose  $\theta$ . Starting from A-NeRF [42] applied to only the real person as a baseline, we introduce our Step 2 + A-NeRF, naive mirror integration, and full mirror integration with and without efficiency-improving extensions.

**A-NeRF initialized by Step 2 (Step 2 + A-NeRF).** To apply articulated neural radiance fields, such as [42] and [43], to our setting, we segment both persons in the image using [26]. We then use the real-mirror person assignment from Step 1 and Step 2 to determine the mask for the real person  $\mathbf{M}$  that contains the 2D keypoints associated to the real person. Our contribution is on how to also include the mirrored person and its mask  $\bar{\mathbf{M}}$ . For the real person, we can apply existing methods, besides minor modifications to run with our skeleton definition. Input is the image  $I$ , skeleton  $\mathbf{v}^{\text{ref}}$ , the bone lengths  $\ell$  and joint angles  $\theta$ . We cast rays to the real person in the scene using pixels  $(u, v)$  within the mask  $\mathbf{M}$ , and query 64 points  $\{\mathbf{b}_k\}_{k=1}^{64}$  along that ray direction  $\mathbf{r} = \mathbf{K}^{-1}(u, v, 1)$  within the 3D bounding box containing the skeleton  $\mathbf{p}$ . By using the skeleton-relative encoding from [42] or [43], we first map the queried points  $\mathbf{b}$  to the local space of each joint using  $T_i$ ,

$$\tilde{\mathbf{b}}_i = T_i^{-1}(\theta_i, \mathbf{v}_i)[\mathbf{b}]. \quad (7)$$

A fully-connected neural network then predicts color  $\gamma_k$  and density  $\sigma_k$  as a function of the transformed queries,  $\gamma_k, \sigma_k = \phi([\tilde{\mathbf{b}}_1, \dots, \tilde{\mathbf{b}}_J])$  for every sample  $k$ . The image is formed by volume rendering, integrating color along the ray while accounting for the transmittance computed from the density, as in the original NeRF.

The objective is the photometric loss  $\mathcal{L}_{\text{Neural}}$  between the generated and observed image, and both the joint angles and parameters of the underlying neural network are optimized jointly. Note that existing articulated NeRF models only apply as we tuned Step 2 to be compatible by introducing the additional smoothness constrained on bone orientation.

**Layered mirror representation.** Mirror occlusion cases, such as the one in Figure 6 where the real and mirrored person overlap, are important, as they result in errors in the



Figure 6. **Occlusion handling.** First, we automatically generate 2D bounding boxes (in grey) from our optimized 3D keypoints. Then we shoot rays (dots) randomly in the intersection area (in green) where occlusions may happen (in yellow).

segmentation masks and can lead to a few but large reconstruction errors. To make occlusion resolution part of the learning process but maintain efficiency, we automatically detect frames where occlusion occurs by measuring the intersection over union (IOU) of the bounding boxes  $\mathbf{N}$  and  $\bar{\mathbf{N}}$  enclosing the projected real and mirrored 3D poses from Section 3.2.

Given these boxes, we compute an intersection box that bounds overlapping areas and shoot rays randomly within the intersection box to resolve occluding pixels. Since each pixel is at an intersection of  $\mathbf{N}$  and  $\bar{\mathbf{N}}$ , we process the occlusion samples along the direct view ray,  $\{\mathbf{b}_k\}_{k=1}^{64}$ , and along its mirrored path,  $\{\bar{\mathbf{b}}_k\}_{k=1}^{64}$ . *Case II* gives the reflected view-ray

$$\bar{\mathbf{r}} = \mathbf{A}_{3 \times 3} \mathbf{r}, \quad (8)$$

with the origin at virtual camera center  $\bar{\mathbf{c}}$ . Note that we do not bound the occlusion samples to  $\mathbf{M}$  and  $\bar{\mathbf{M}}$  as the segmentation masks are often unreliable when people overlap.

Furthermore, sampling a different number of samples for occlusion rays does not fare well with the batch processing in NeRF. To make it compatible, we process real and mirror samples, including occlusion cases, independently to yield image layers  $\mathbf{L}$  and  $\bar{\mathbf{L}}$  and corresponding alpha maps  $\alpha$  and  $\bar{\alpha}$ . We exploit that if occlusion happens, the real person occludes the mirrored person. This holds in general, since the mirror image results from an indirect light path that is always longer than the direct view, and enables combining these partial results using back-to-front layering. Starting from the background image  $I_{\text{bg}}$ , the final image is

$$\hat{\mathbf{I}} = \mathbf{L}\alpha + (1 - \alpha)(\bar{\mathbf{L}}\bar{\alpha} + (1 - \bar{\alpha})I_{\text{bg}}). \quad (9)$$

This layered composition enables efficient training on  $\mathcal{L}_{\text{Neural}}$  and rendering in batches of the same size, while accounting for mirror occlusion.

**Baseline w/o layering.** Without the introduced layering, it would require to sample twice as many points over the union of both masks  $\mathbf{M}$  and  $\bar{\mathbf{M}}$ , the samples  $\{\mathbf{b}_k\}_{k=1}^{64}$  along

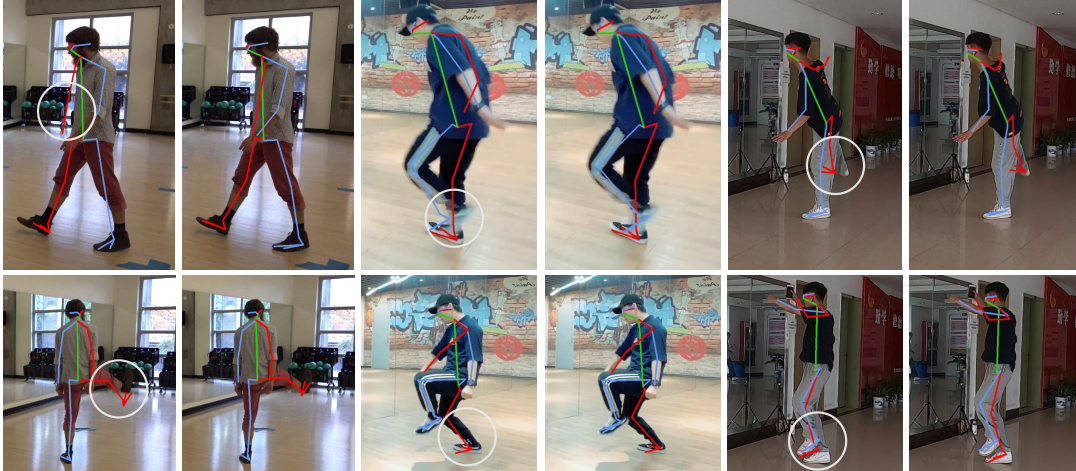


Figure 7. **Qualitative results of pose refinement on a new diverse sequence, internet video, and *MirrorHuman-eval* dataset [8] respectively.** Our Mirror A-NeRF aligns the skeleton model well to the images. **Left:** Before refinement (after Step 2) **Right:** After the volumetric model refinement (Step 3).

the ray up to the mirror and samples  $\{\bar{\mathbf{b}}_k\}_{k=1}^{64}$  after the mirror reflection. However, unless real and mirrored person occlude, one of the two sample sets is in empty space, thereby training NeRF to merely predict 0 density for that set, leading to slow convergence.

**Baseline w/o occlusion** Assuming that the person masks  $\mathbf{M}$  and  $\bar{\mathbf{M}}$  are correct and non-overlapping, one can render two separate images of real and mirror person by respectively sampling  $\mathbf{M}$  and  $\bar{\mathbf{M}}$ , using *Case II* with the notion of two cameras. By minimizing the photometric objective, this baseline is efficient and utilizes the information across both views but does not account for mirror occlusions and imperfect masks around occlusion areas.

## 4. Evaluation

We compare our Mirror-aware Neural Human on the tasks of body pose and appearance reconstruction against state-of-the-art methods to verify that existing NeRF-based body models benefit largely from the additional geometric mirror constraints, that every stage of our motion capture pipeline brings improvement, and ablate model choices. The supplemental document and video provide additional examples.

**Variants and Baselines.** We integrated our *Mirror-aware Neural Human* formulation into A-NeRF [42] and DANBO [43] and refer to them as *Mirror A-NeRF* and *Mirror DANBO*. We use the original A-NeRF [42] and DANBO [43] as baselines, as well as the mirror-based pose estimation method, MirrorHuman [8] and the established single-view reconstruction techniques SPIN [22] and SM-PLify [34]. For pose estimation accuracy, we only compare to the A-NeRF neural body method as DANBO does not

support pose refinement.

**Benchmark Datasets.** We use the *MirrorHuman-eval* dataset from [8]. It contains a complex dancing performance in front of a large mirror and is captured with six cameras arranged in an arc around the mirror. We exclude camera 4 as it is directly frontal to the mirror and leads to degenerate configuration where the mirrored person is largely occluded. Since no validation set was specified, we use camera 2 and 3, that are placed between a 45-to-90 degree angle to the mirror, for tuning hyperparameters and test on all cameras as previous methods did. Following [8], we optimize the pose separately for each video, treating this dataset as five independent recordings instead of a multi-view setup. We also concur in evaluating pose accuracy for Step 2 and 3 on every 100th frame while reconstructing in-between frames only to ensure smoothness. For the neural models, we quantify image reconstruction accuracy on every 20th frame and withhold the last 10% of frames to test novel pose synthesis.

**Additional qualitative sequences.** To be able to demonstrate generality and showcase the simplicity of capturing with a mirror, we utilize the internet dancing recordings from [8] and recorded a new dataset that is more diverse in terms of appearance, e.g., including a beard, male and female, loose clothing, and casual everyday motions that go beyond dancing (see Figure 7). We used a single camera for recording and employed 2000 frames for reconstruction.

**Metrics.** For pose estimation tasks, we report the scale-normalized MPJPE (N-MPJPE) introduced in [37], and the Procrustes-aligned MPJPE (PA-MPJPE), both in mm over the 15 joints defined in [8]. We omit MPJPE without scale normalization as monocular reconstruction is inherently scale-ambiguous [13]. For image synthesis, we quan-

Method	3D Training	Mirror Calibration	2D Input	PA-MPJPE ↓
SMPLify-X [34]	3D pose prior	n/a	detections	90.57
A-NeRF [42]	partial (init.)	n/a	detections	84.72
SPIN [22]	supervised	n/a	detections	67.42
SPIN [22]+SMPLify [34]	partial (init.)	n/a	detections	<b>61.47</b>
Ours (Step 2)	unsupervised	automatic	detections	63.00
Ours (Step 2 + A-NeRF [42])	unsupervised	automatic	detections	62.69
Ours (Step 3, w/o occlusion)	unsupervised	automatic	detections	61.46
Ours (Step 3, w occlusion)	unsupervised	automatic	detections	<b>61.30</b>
Ours (Step 2, using GT input)	unsupervised	automatic	manual	39.53
MirrorHuman [8] (w/o mirror GT)	partial (init.)	automatic	manual	33.24
MirrorHuman [8]	partial (init.)	manual	manual	<b>32.96</b>

Table 1. **3D pose reconstruction.** Ours is the only fully-automatic mirror-based method. We match the accuracy of off-the-shelf 3D pose estimators with only 2D detections as input and reproduce results of mirror methods using GT input [8].

Method	Cam 6 PSNR ↑	Cam 6 SSIM ↑
A-NeRF [42]	25.52	0.8662
Ours(Mirror A-NeRF w/o Occlusion)	<b>25.89</b>	<b>0.9210</b>
DANBO [43]	28.97	0.9193
Ours(Mirror DANBO w/o Occlusion)	<b>31.87</b>	<b>0.9522</b>

Table 2. **Quantitative image reconstruction accuracy** on *MirrorHuman-eval* dataset in terms of PSNR and SSIM. A-NeRF [42] and DANBO [43] without mirror remain blurry, leading to lower scores.

tify the image quality by PSNR and SSIM [51].

**Implementation details.** In Step 2, we optimize 3D poses for 2K iterations. For Step 3, we train the neural rendering model up to a maximum of 300K steps for DANBO and a maximum of  $2 \times 200K$  for A-NeRF with pose refinement and appearance fine-tuning.

#### 4.1. Mirror Normal Estimation

Our average normal estimation error (using 2D detections as input) is  $0.4^\circ$  compared to the GT normal provided in [8]. Camera 4 is excluded as the real person occludes the mirror image in most frames. This automatic mirror calibration is highly accurate and very close to the  $0.5^\circ$  obtained from the vanishing point method in [8] on the same cameras.

#### 4.2. Pose Estimation

**Comparison to refining pose with a dense body model.** Table 1 shows the results for the *MirrorHuman-eval* dataset. Compared to A-NeRF [42], which also refines SPIN estimates using a volumetric body model, our method improves 3D pose estimates significantly, by more than 20%. This highlights the importance of integrating a second view for accurate reconstruction, here via the mirror. Figure 7 shows that, by benefiting from the NeRF model, the joint refinement of pose and shape improves significantly, particularly on extreme poses.

**Comparison to methods lifting 2D pose to 3D.** We outperform the supervised approach SPIN [22] and single-view optimization SMPLify-X [34], and match their combina-

tion, as these single-view approaches do not fare well under occlusion and are prone to depth ambiguity.

**Comparison to existing mirror approaches.** The prior method [8] focuses on controlled conditions, using manually corrected 2D ground-truth (GT) and a pre-trained pose estimator for initialization. To compare on fair grounds, we run a variant that also uses 2D GT as input. Table 1 shows that it matches the accuracy up to 7mm. The remaining discrepancy can be attributed to our method not being tuned for GT input and not using a 3D pose estimator, which are known to not generalize well to very extreme motions. The other existing mirror work [27] cannot be compared to as it does not provide joint angles for shape reconstruction and does not evaluate on publicly available datasets.

#### 4.3. Body Shape and Appearance

Figure 1 and Figure 8 show the images synthesized by different neural rendering models. For better visualization, we apply connected component analysis to remove floating artefacts stemming from shadowing and background. On *MirrorHuman-eval dataset* [8], both of our variants, Mirror A-NeRF and Mirror DANBO, synthesize sharper results with more fine-grained details compared to the mirror-less counterparts. We attribute the improvement to the better pose initialization from Step 2 and the additional appearance supervision by the mirror view, all enabled by our mirror modeling. Table 2 validates the visual improvement quantitatively in terms of image reconstruction accuracy. Both Mirror A-NeRF and Mirror DANBO better learn the body shape and appearance, verifying the effectiveness of our *Mirror-aware Neural Humans*.

#### 4.4. Ablation Study

To analyze the effect of our model choices in Step 2, we use camera 3 in the *MirrorHuman-eval* dataset over all 19 joints that have ground truth. We perform experiments with different configurations for the joint optimization of the bone factors, global position, and mirror parameters. Table 3 validates that each component contributes to the final result. The effect of and robustness to different weights of the

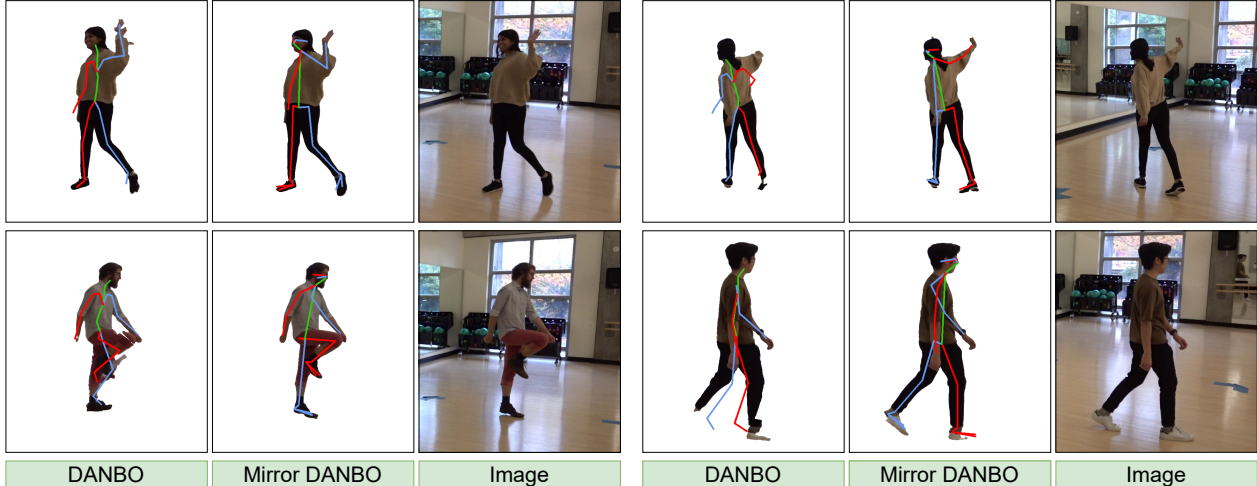


Figure 8. **Neural body reconstruction** on three different subjects from the additional qualitative sequences, including loose clothing, challenging poses, and casual day-to-day motion. Our Mirror-Aware Neural Humans reconstructs the body details considerably benefiting from the mirror model and skeleton.

smoothness terms are evaluated and explained in the supplemental material.

We also analyze the different ways of integrating mirror constraints and occlusion handling on cameras 6 and 7. Table 4 presents the pose refinement outcomes after the neural rendering steps (Section 3.3). Running A-NeRF with our Step 2 poses already improves due to the more accurate pose initialization. Our Mirror A-NeRF further improves, as it enables pixel-level multi-view (real and mirror pose) refinement. Taking occlusion into account further surpasses the two baselines. Note that the total improvement of handling occlusions computed over all frames and all joints is small and we therefore only enable it on sequences that include a sufficient number of occlusion frames.

Components removed from model	N-MPJPE ↓	PA-MPJPE ↓
Base w/o smooth. and feet constr.	99.94	63.03
w/o location smooth.	93.79	57.98
w/o orientation smooth.	92.88	57.93
w/o feet constraint	84.73	54.06
Full objective	<b>62.45</b>	<b>44.15</b>

Table 3. **Ablation study** on the optimal regularization configuration to reduce the influence of noisy detections. All our contributions improve on the baseline.

Method	Cam 6 PA-MPJPE ↓	Cam 7 PA-MPJPE ↓
A-NeRF [42]	86.21	89.10
Ours (Step 2 + A-NeRF)	51.21	58.61
Ours (Mirror A-NeRF)	48.84	57.82
Ours (Mirror A-NeRF w/ occlusion)	<b>48.51</b>	<b>57.32</b>

Table 4. **Pose refinement on MirrorHuman-eval dataset [5] on videos with occlusions.** With occlusion handling, Mirror-Aware Neural Humans improves upon A-NeRF [42].

## 5. Limitations and Future Work

Our 3D reconstruction algorithm only works in cases where the person’s mirror image is visible most of the time, restricting the camera placement close to 20-to-70 degrees to the mirror. When the camera view direction is close to parallel or orthogonal to the mirror, 3D triangulation is unreliable. Moreover, the 3D reconstruction is sensitive to the initial reconstruction of the ground plane and focal length, e.g., errors emerging when bystanders with varying heights violate the constant height assumption.

Moreover, since we rely on an estimated segmentation mask, sometimes body parts are cut out or the shadow or other background parts in the scene are represented in the 3D volumetric model creating opportunities for future work. In the future, we will attempt to apply similar techniques to animal motion capture, which, however, requires redefining our upright standing assumption and filtering in Step 1.

## 6. Conclusion

Our method reconstructs a 3D neural body model from mirror images by treating the mirror as a second camera and calibrating the camera extrinsics and mirror geometry directly from the motion of people detected in 2D. This alleviates manual mirror annotation and initializing with pre-trained models, which lets us reconstruct difficult and complex human performances for which existing approaches struggle.

Mirror-Aware Neural Humans let anyone with a mirror and camera reconstruct a full 3D human model. In particular, we foresee low-cost medical applications, such as mirror-based pose estimation for rehabilitation [25].



## References

- [1] Abdullah Akay and Yusuf Sinan Akgul. 3D reconstruction with mirrors and RGB-D cameras. In *International Conference on Computer Vision Theory and Applications*, pages 325–334. IEEE, 2014. [2](#)
- [2] Thiemo Alldieck, Marcus Magnor, Bharat Lal Bhatnagar, Christian Theobalt, and Gerard Pons-Moll. Learning to reconstruct people in clothing from a single RGB camera. In *Proceedings of the IEEE/CVF Conference on Computer Vision and Pattern Recognition*, pages 1175–1186, 2019. [1](#)
- [3] Anonymous. CasCalib: Cascaded Calibration for Motion Capture from Sparse Unsynchronized Cameras. *Supplemental document*, 2023. [3](#)
- [4] Zhihua Chen, Xiaoli Liu, Bing Sheng, and Ping Li. GAR-Net: Graph attention residual networks based on adversarial learning for 3D human pose estimation. In *Computer Graphics International Conference*, pages 276–287. Springer, 2020. [2](#)
- [5] Hao-Shu Fang, Shuqin Xie, Yu-Wing Tai, and Cewu Lu. RMPE: Regional multi-person pose estimation. In *Proceedings of the IEEE International Conference on Computer Vision*, pages 2334–2343, 2017. [8](#)
- [6] Hao-Shu Fang, Jiefeng Li, Hongyang Tang, Chao Xu, Haoyi Zhu, Yuliang Xiu, Yong-Lu Li, and Cewu Lu. Alpha-pose: Whole-body regional multi-person pose estimation and tracking in real-time. *IEEE Transactions on Pattern Analysis and Machine Intelligence*, 2022. [2](#)
- [7] Qi Fang, Qing Shuai, Junting Dong, Hujun Bao, and Xiaowei Zhou. Supplementary Material: Reconstructing 3D Human Pose by Watching Humans in the Mirror. [https://zju3dv.github.io/Mirrored-Human/images/mirror\\_supp.pdf](https://zju3dv.github.io/Mirrored-Human/images/mirror_supp.pdf). Accessed: 2023-08-03. [2](#)
- [8] Qi Fang, Qing Shuai, Junting Dong, Hujun Bao, and Xiaowei Zhou. Reconstructing 3D human pose by watching humans in the mirror. In *Proceedings of the IEEE/CVF Conference on Computer Vision and Pattern Recognition*, pages 12814–12823, 2021. [1](#), [2](#), [6](#), [7](#)
- [9] Xiaohan Fei, Henry Wang, Lin Lee Cheong, Xiangyu Zeng, Meng Wang, and Joseph Tighe. Single view physical distance estimation using human pose. In *Proceedings of the IEEE/CVF International Conference on Computer Vision*, pages 12406–12416, 2021. [2](#), [3](#)
- [10] Mohsen Gholami, Bastian Wandt, Helge Rhodin, Rabab Ward, and Z Jane Wang. AdaptPose: Cross-dataset adaptation for 3D human pose estimation by learnable motion generation. In *Proceedings of the IEEE/CVF Conference on Computer Vision and Pattern Recognition*, pages 13075–13085, 2022. [2](#)
- [11] Kehong Gong, Jianfeng Zhang, and Jiashi Feng. PoseAug: A differentiable pose augmentation framework for 3D human pose estimation. In *Proceedings of the IEEE/CVF Conference on Computer Vision and Pattern Recognition*, pages 8575–8584, 2021.
- [12] Shanyan Guan, Jingwei Xu, Yunbo Wang, Bingbing Ni, and Xiaokang Yang. Bilevel online adaptation for out-of-domain human mesh reconstruction. In *Proceedings of the IEEE/CVF Conference on Computer Vision and Pattern Recognition*, pages 10472–10481, 2021. [2](#)
- [13] Semih Gunel, Helge Rhodin, and Pascal Fua. What face and body shapes can tell us about height. In *Proceedings of the IEEE/CVF International Conference on Computer Vision Workshops*, pages 0–0, 2019. [6](#)
- [14] Julian Habekost, Takaaki Shiratori, Yuting Ye, Taku Komura, Mingyi Shi, Kfir Aberman, Andreas Aristidou, Dani Lischinski, Daniel Cohen-Or, Baoquan Chen, et al. Learning 3D global human motion estimation from unpaired, disjoint datasets. In *British Machine Vision Conference*. BMVC, 2020. [2](#)
- [15] Marc Habermann, Weipeng Xu, Michael Zollhoefer, Gerard Pons-Moll, and Christian Theobalt. LiveCap: Real-time human performance capture from monocular video. *ACM Transactions On Graphics*, 38(2):1–17, 2019. [1](#)
- [16] Ikhsanul Habibie, Weipeng Xu, Dushyant Mehta, Gerard Pons-Moll, and Christian Theobalt. In the wild human pose estimation using explicit 2D features and intermediate 3D representations. In *Proceedings of the IEEE/CVF Conference on Computer Vision and Pattern Recognition*, pages 10905–10914, 2019. [2](#)
- [17] B. Hu, Christopher M. Brown, and R. Nelson. Multiple-view 3-D reconstruction using a mirror. In *Technical Report 863 Computer Science Department*. The University of Rochester, 2005. [2](#)
- [18] Catalin Ionescu, Fuxin Li, and Cristian Sminchisescu. Latent structured models for human pose estimation. In *2011 International Conference on Computer Vision*, pages 2220–2227. IEEE, 2011. [3](#)
- [19] Catalin Ionescu, Dragos Papava, Vlad Olaru, and Cristian Sminchisescu. Human3.6m: Large scale datasets and predictive methods for 3d human sensing in natural environments. *IEEE transactions on pattern analysis and machine intelligence*, 36(7):1325–1339, 2013. [3](#)
- [20] Umar Iqbal, Pavlo Molchanov, and Jan Kautz. Weakly-supervised 3D human pose learning via multi-view images in the wild. In *Proceedings of the IEEE/CVF Conference on Computer Vision and Pattern Recognition*, pages 5243–5252, 2020. [2](#)
- [21] Muhammed Kocabas, Salih Karagoz, and Emre Akbas. Self-supervised learning of 3D human pose using multi-view geometry. In *Proceedings of the IEEE/CVF Conference on Computer Vision and Pattern Recognition*, pages 1077–1086, 2019. [2](#)
- [22] Nikos Kolotouros, Georgios Pavlakos, Michael J Black, and Kostas Daniilidis. Learning to reconstruct 3D human pose and shape via model-fitting in the loop. In *Proceedings of the IEEE/CVF International Conference on Computer Vision*, pages 2252–2261, 2019. [6](#), [7](#)
- [23] Emőd Kovács. Rotation about an arbitrary axis and reflection through an arbitrary plane. In *Annales Mathematicae et Informaticae*, pages 175–186, 2012. [3](#)
- [24] Jogendra Nath Kundu, Siddharth Seth, Varun Jampani, Mugalodi Rakesh, R Venkatesh Babu, and Anirban Chakraborty. Self-supervised 3D human pose estimation via part guided novel image synthesis. In *Proceedings of the IEEE/CVF*

- Conference on Computer Vision and Pattern Recognition*, pages 6152–6162, 2020. [2](#)
- [25] Seokjun Lee and Soon Ki Jung. Legs pose estimation using a planar mirror for a rehabilitation training system. *Korean Multimedia Society International Conference*, pages 106–109, 2011. [8](#)
- [26] Shanchuan Lin, Linjie Yang, Imran Saleemi, and Soumyadip Sengupta. Robust high-resolution video matting with temporal guidance. In *Proceedings of the IEEE/CVF Winter Conference on Applications of Computer Vision*, pages 238–247, 2022. [5](#)
- [27] Chenchen Liu, Yongzhi Li, Kangqi Ma, Duo Zhang, Peijun Bao, and Yadong Mu. Learning 3-D human pose estimation from catadioptric videos. In *International Joint Conference on Artificial Intelligence*, pages 852–859, 2021. [1](#), [2](#), [3](#), [7](#)
- [28] Dushyant Mehta, Helge Rhodin, Dan Casas, Pascal Fua, Oleksandr Sotnychenko, Weipeng Xu, and Christian Theobalt. Monocular 3D human pose estimation in the wild using improved cnn supervision. In *International Conference on 3D Vision*, pages 506–516. IEEE, 2017. [2](#)
- [29] Dushyant Mehta, Srinath Sridhar, Oleksandr Sotnychenko, Helge Rhodin, Mohammad Shafiei, Hans-Peter Seidel, Weipeng Xu, Dan Casas, and Christian Theobalt. VNect: Real-time 3D human pose estimation with a single RGB camera. *ACM Transactions on Graphics*, 36(4):1–14, 2017. [2](#)
- [30] Rahul Mitra, Nitesh B Gundavarapu, Abhishek Sharma, and Arjun Jain. Multiview-consistent semi-supervised learning for 3D human pose estimation. In *Proceedings of the IEEE/CVF Conference on Computer Vision and Pattern Recognition*, pages 6907–6916, 2020. [1](#), [2](#)
- [31] Sameer A Nene and Shree K Nayar. Stereo with mirrors. In *Sixth International Conference on Computer Vision (IEEE Cat. No. 98CH36271)*, pages 1087–1094. IEEE, 1998. [2](#)
- [32] Trong-Nguyen Nguyen, Huu-Hung Huynh, and Jean Meunier. 3D reconstruction with time-of-flight depth camera and multiple mirrors. *IEEE Access*, 6:38106–38114, 2018. [2](#)
- [33] Qiang Nie, Ziwei Liu, and Yunhui Liu. Unsupervised 3D human pose representation with viewpoint and pose disentanglement. In *European Conference on Computer Vision*, pages 102–118. Springer, 2020. [1](#), [2](#)
- [34] Georgios Pavlakos, Vasileios Choutas, Nima Ghorbani, Timo Bolkart, Ahmed AA Osman, Dimitrios Tzionas, and Michael J Black. Expressive body capture: 3D hands, face, and body from a single image. In *Proceedings of the IEEE/CVF Conference on Computer Vision and Pattern Recognition*, pages 10975–10985, 2019. [6](#), [7](#)
- [35] Dario Pavlo, Christoph Feichtenhofer, David Grangier, and Michael Auli. 3D human pose estimation in video with temporal convolutions and semi-supervised training. In *Proceedings of the IEEE/CVF Conference on Computer Vision and Pattern Recognition*, pages 7753–7762, 2019. [2](#)
- [36] Ilya Reshetouski and Ivo Ihrke. Mirrors in computer graphics, computer vision and time-of-flight imaging. In *Time-of-Flight and Depth Imaging. Sensors, Algorithms, and Applications*, pages 77–104. Springer, 2013. [2](#)
- [37] Helge Rhodin, Mathieu Salzmann, and Pascal Fua. Unsupervised geometry-aware representation for 3D human pose estimation. In *Proceedings of the European Conference on Computer Vision*, pages 750–767, 2018. [1](#), [2](#), [6](#)
- [38] Helge Rhodin, Jörg Spörri, Isinsu Katircioglu, Victor Constantin, Frédéric Meyer, Erich Müller, Mathieu Salzmann, and Pascal Fua. Learning monocular 3D human pose estimation from multi-view images. In *Proceedings of the IEEE Conference on Computer Vision and Pattern Recognition*, pages 8437–8446, 2018.
- [39] Helge Rhodin, Victor Constantin, Isinsu Katircioglu, Mathieu Salzmann, and Pascal Fua. Neural scene decomposition for multi-person motion capture. In *Proceedings of the IEEE/CVF Conference on Computer Vision and Pattern Recognition*, pages 7703–7713, 2019. [1](#), [2](#)
- [40] Guillaume Rochette, Chris Russell, and Richard Bowden. Weakly-supervised 3D pose estimation from a single image using multi-view consistency. In *Proceedings of the 30th British Machine Vision Conference. BMVC*, 2019. [2](#)
- [41] Katie Schwartz. Field guide to optomechanical design and analysis. Society of Photo-Optical Instrumentation Engineers, 2012. [3](#)
- [42] Shih-Yang Su, Frank Yu, Michael Zollhöfer, and Helge Rhodin. A-NeRF: Articulated neural radiance fields for learning human shape, appearance, and pose. In *Advances in Neural Information Processing Systems*, 2021. [1](#), [2](#), [5](#), [6](#), [7](#), [8](#)
- [43] Shih-Yang Su, Timur Bagautdinov, and Helge Rhodin. DANBO: Disentangled articulated neural body representations via graph neural networks. *arXiv preprint arXiv:2205.01666*, 2022. [1](#), [2](#), [5](#), [6](#), [7](#)
- [44] Jennifer J Sun, Jiaping Zhao, Liang-Chieh Chen, Florian Schroff, Hartwig Adam, and Ting Liu. View-invariant probabilistic embedding for human pose. In *European Conference on Computer Vision*, pages 53–70. Springer, 2020. [1](#), [2](#)
- [45] Kosuke Takahashi, Shohei Nobuhara, and Takashi Matsuyama. A new mirror-based extrinsic camera calibration using an orthogonality constraint. In *IEEE Conference on Computer Vision and Pattern Recognition*, pages 1051–1058. IEEE, 2012. [2](#)
- [46] Zheng Tang, Yen-Shuo Lin, Kuan-Hui Lee, Jenq-Neng Hwang, Jen-Hui Chuang, and Zhijun Fang. Camera self-calibration from tracking of moving persons. In *2016 23rd International Conference on Pattern Recognition (ICPR)*, pages 265–270. IEEE, 2016. [2](#)
- [47] Bastian Wandt and Bodo Rosenhahn. RepNet: Weakly supervised training of an adversarial reprojection network for 3D human pose estimation. In *Proceedings of the IEEE/CVF Conference on Computer Vision and Pattern Recognition*, pages 7782–7791, 2019. [2](#)
- [48] Bastian Wandt, Marco Rudolph, Petrisa Zell, Helge Rhodin, and Bodo Rosenhahn. CanonPose: Self-supervised monocular 3D human pose estimation in the wild. In *Proceedings of the IEEE/CVF Conference on Computer Vision and Pattern Recognition*, pages 13294–13304, 2021. [1](#), [2](#)
- [49] Bastian Wandt, James J Little, and Helge Rhodin. ElePose: Unsupervised 3D human pose estimation by predicting camera elevation and learning normalizing flows on 2D poses. In *Proceedings of the IEEE/CVF Conference on Computer Vision and Pattern Recognition*, pages 6635–6645, 2022. [2](#)

- [50] Chaoyang Wang, Chen Kong, and Simon Lucey. Distill knowledge from NRSfM for weakly supervised 3D pose learning. In *Proceedings of the IEEE/CVF International Conference on Computer Vision*, pages 743–752, 2019. 2
- [51] Zhou Wang, Alan C Bovik, Hamid R Sheikh, and Eero P Simoncelli. Image quality assessment: From error visibility to structural similarity. *IEEE Transactions on Image Processing*, 13(4):600–612, 2004. 7
- [52] Chung-Yi Weng, Brian Curless, Pratul P Srinivasan, Jonathan T Barron, and Ira Kemelmacher-Shlizerman. HumanNeRF: Free-viewpoint rendering of moving people from monocular video. In *Proceedings of the IEEE/CVF Conference on Computer Vision and Pattern Recognition*, pages 16210–16220, 2022. 1
- [53] Yufei Xu, Jing Zhang, Qiming Zhang, and Dacheng Tao. Vit-pose: Simple vision transformer baselines for human pose estimation. *Advances in Neural Information Processing Systems*, 35:38571–38584, 2022. 2
- [54] Gengshan Yang, Minh Vo, Natalia Neverova, Deva Ramanan, Andrea Vedaldi, and Hanbyul Joo. BANMo: Building animatable 3D neural models from many casual videos. In *Proceedings of the IEEE/CVF Conference on Computer Vision and Pattern Recognition*, pages 2863–2873, 2022. 1
- [55] Ze-Xin Yin, Jiaxiong Qiu, Ming-Ming Cheng, and Bo Ren. Multi-space neural radiance fields. In *Proceedings of the IEEE/CVF Conference on Computer Vision and Pattern Recognition*, pages 12407–12416, 2023. 2
- [56] Andrei Zanfir, Eduard Gabriel Bazavan, Hongyi Xu, William T Freeman, Rahul Sukthankar, and Cristian Sminchisescu. Weakly supervised 3D human pose and shape reconstruction with normalizing flows. In *European Conference on Computer Vision*, pages 465–481. Springer, 2020. 2
- [57] Yi Zhou, Connelly Barnes, Jingwan Lu, Jimei Yang, and Hao Li. On the continuity of rotation representations in neural networks. In *Proceedings of the IEEE/CVF Conference on Computer Vision and Pattern Recognition*, pages 5745–5753, 2019. 3